ACS OMEGA

http://pubs.acs.org/journal/acsodf

Article

Topological Nodal Surface and Quadratic Dirac Semimetal States and van Hove Singularities in ScH_3 and LuH_3 Superconductors

Ali Sufyan* and J. Andreas Larsson

Cite This: *ACS Omega* 2023, 8, 9607−9613

Read Online

ACCESS | Metrics & More | Article Recommendations | Supporting Information

ABSTRACT: The coexistence of non-trivial topology and superconductivity in a material may induce a novel physical phenomenon known as topological superconductivity. Topological superconductors have been the subject of intense research, yet there are severe limitations in their application due to a lack of suitable materials. Topological nodal surface semimetals with nearly flat nodal surfaces near the Fermi level can be promising materials to achieve topological superconductivity. Here, we use first-principles calculations to examine the topological electronic characteristics of two new superconductors, ScH_3 and LuH_3, at both ambient and high pressures. Our studies show that both ScH_3 and LuH_3 have van Hove singularities, which confirms their superconductivity. Interestingly, both materials host topological nodal surface states under the protection of time reversal and spatial inversion symmetries in the absence of spin−orbit coupling (SOC). These nodal surfaces are distinguished by a pair of unique drum-head-like surface states not previously observed in nodal surface semimetals. Moreover, the nodal surfaces transform into essential spin−orbit quadratic Dirac points when SOC is included. Our findings demonstrate that ScH_3 and LuH_3 are good candidates to investigate the exotic properties of both nodal surface semimetals (NSSMs) and quadratic Dirac semimetal states and also provide a platform to explore the coexistence of topology and superconductivity in NSSMs with promising applications in high-speed electronics and topological quantum computing.

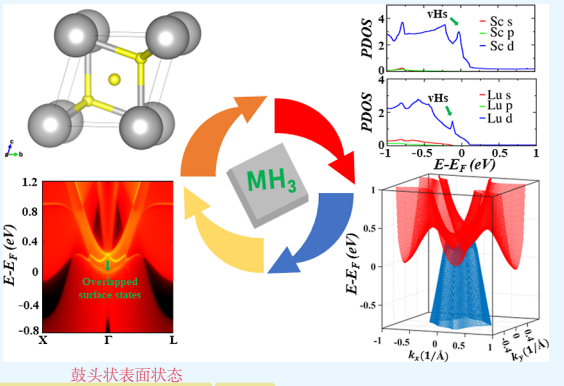

鼓头状表面状态

INTRODUCTION

During the past decade, topological states of matter have emerged as a major area of research in condensed matter physics.[1−3] With inspiration from earlier work on topological insulators,[4−16] the research focus is now shifting toward gapless topological phases, particularly topological semimetals (TSMs).[17−22] TSMs exhibit nontrivial band crossings (BCs) between valence and conduction bands in momentum space protected by certain symmetries, such that the quasiparticles behave drastically different from the conventional Schrödinger-type fermions. For instance, in Dirac[23−26] and Weyl semimetals,[27−30] the zero-dimension (0D) BCs between conduction and valence bands, accompanied by fourfold and twofold degeneracies, occur at isolated k points around which the low-energy quasiparticles resemble relativistic Dirac and Weyl fermions, allowing high-energy physics to be simulated in a desktop setting. In addition to Weyl/Dirac SMs, nodal line semimetals[31−39] (NLSMs) form another class of SMs that host 1D BCs and have also been extensively pursued over the past few years. Recently, a new class of SMs referred to as nodal surface semimetals[40,41] (NSSMs) has also been proposed, initially by Zhong et al.[42] and Liang et al.[43] in carbon networks and $BaVS_3$ family materials, respectively.

NSSMs possess 2D BCs, where each point on the surface is a crossing point between conduction and valence bands with linear dispersion along the surface normal direction.[40] Wu et al.[40] divide NSSMs into two categories based on symmetry protection mechanisms and also provide sufficient conditions and examples for robust NSSMs under spin−orbit coupling (SOC) and in magnetic materials. However, the proposed NSSMs are far fewer than Weyl-Dirac and NLSMs, and the number is even smaller when it comes to their experimental realization.[44−48] NSSMs are anticipated to hold interesting topological physics and many promising applications in devices. To study these properties from a material point of view, it is crucial that the band degeneracies are close to the Fermi level. Moreover, for experimental realization, the material should be stable and easy to synthesize. These rigorous conditions limit the development of suitable NSSMs, and there is an urgent need to search for realistic materials that are suitable for the experimental study of NSSM states.

In parallel, topological superconductors have attracted much attention in recent years because they can host Majorana zero modes and have potential applications in topological quantum

Received: January 11, 2023
Accepted: February 20, 2023
Published: March 1, 2023

computation.[49−53] Despite great efforts to develop topological superconductors, here a severe shortage of suitable materials has hindered their development.[50] Experimentally, doping a topological material to turn it into a superconductor or tuning a superconducting material into a topological phase via doping are common methods to realize new topological superconductors.[54−57] In addition, topological superconductivity can also be achieved by topological materials that can be driven into a superconducting phase by pressure.[58,59] However, the ideal approach to realize new topological superconductors is to find a single material that possesses both topological and superconducting properties simultaneously.[60−66]

Polyhydrides are a large class of materials that have undergone extensive research in a variety of fields, including energy storage[67] and superconductivity.[68−72] The chemical precompression of polyhydrides makes them an excellent candidate for high-temperature superconductors at feasible pressures.[73] Rare-earth metal hydrides LaH_{10} and YH_{10} are predicted to be surprising high-temperature superconductors at megabar pressures,[74−78] and several rare-earth metal hydrides, including CeH_9,[79] CeH_{10},[79] YH_6,[80] and YH_9,[81] have been experimentally demonstrated to be superconductors with promisingly high T_c. Recently, two new hydrides, ScH_3 and LuH_3, have also been experimentally synthesized and found to exhibit superconductivity, with $T_c \sim 18.5$ K at 131 GPa and 12.4 K at 122 GPa,[82] respectively. ScH_3 and LuH_3 are the only REH_3 hydrides whose superconducting properties have been experimentally confirmed. Despite the fact that both of these hydrides show promise for superconductivity, research on their electronic topological properties has yet to be done.

For the aforementioned reasons, we have examined the topological features of superconducting hydrides, ScH_3 and LuH_3[82] at both ambient and high pressures in the present study. Our first-principles calculations show that these materials exhibit U-shaped nodal surface states in the absence of SOC. When SOC is included, the nodal surface states split and transform into an essential quadratic Dirac cone[83] that is located very close to the Fermi level. Furthermore, we also identified the presence of van Hove singularities (vHss) in ScH_3 and LuH_3, which verifies the superconductive nature of these materials. Thus, our work provides a promising material platform for exploring the intriguing properties of the nodal surface and quadratic Dirac semimetal states, as well as new candidates exhibiting topological and superconducting properties simultaneously.

COMPUTATIONAL DETAILS

First-principles calculations based on density functional theory[84] were performed using the projector augmented wave[85] method as implemented in the Vienna ab initio simulation (VASP)[86,87] package. The exchange−correlation functional was treated using the Perdew−Burke−Ernzerhof generalized gradient approximation (GGA)[88] with the cutoff energy set to 450 eV. The Brillouin-zone (BZ) integration was sampled using 18 × 18 × 18 Γ-centered Monkhorst−Pack grids.[89] The structures were relaxed until the residual force on each atom was less than 10^{-3} eV/Å. The energy convergence criterion for electronic structure calculations was set to 10^{-6} eV. The SCAN[90] meta-GGA energy functional was used to correct the underestimated band gaps under GGA. The raw output files of VASP were extracted and analyzed using the VASPKIT code.[91] The real-space tight-binding model Hamiltonians were constructed by using the VASP2WANNIER90 interface,[92] and Sc/Lu d and H s states were included in generating Wannier functions. The surface electronic structures were calculated using the WannierTools package.[93]

RESULTS AND DISCUSSION

Both scandium and lutetium tri-hydrides crystallize in a cubic configuration with the space group $Fm3\_m$ (no. 225). The primitive unit cell of these trihydrides includes one Sc/La atom and three H atoms, as shown in Figure 1a. The Sc/Lu atom is located at (0, 0, 0), while the H atoms are located at (0.25, 0.25, 0.25), (0.75, 0.75, 0.75), and (0.5, 0.5, 0.5) positions. Since it has been reported that these compounds exhibit superconductivity at 131 and 122 GPa,[82] respectively, their electronic and topological properties have been simulated at both ambient and high pressures (131 GPa for ScH_3 and 122 GPa for LuH_3). Both compounds display similar electronic and topological properties at ambient and high pressure; the ambient-pressure results will be discussed here, whereas the high-pressure results are given in the Supporting Information. The calculated lattice parameters at ambient pressure for ScH_3 and LuH_3 are $a = b = c = 3.36$ Å and 3.53 Å, respectively, and the cell angles are $\alpha = \beta = \gamma = 60°$. Furthermore, the crystal structure possesses inversion symmetry and also respects time-reversal symmetry. Figure 1b displays the corresponding BZ with high-symmetry points.

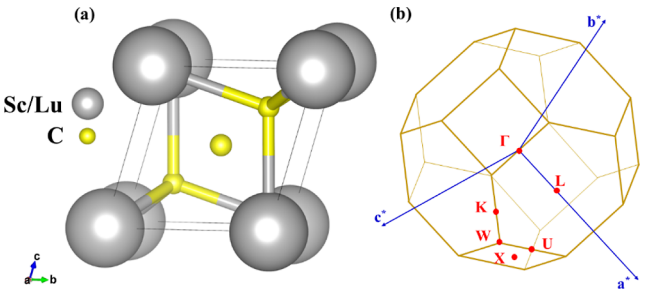

Figure 1. (a) Side view of the crystal structure. The gray and yellow spheres represent the Sc/Lu and H atoms, respectively. (b) Corresponding bulk BZ.

The calculated SCAN electronic band structures for ScH_3 and LuH_3 are given in Figure 2a,c, respectively, in the absence of SOC. In both materials, the bands are mostly confined to two regions labeled as B1 and B2 and share similar semimetallic characteristics. Near the Fermi level, the conduction band maximum (CBM) and valence band minimum (VBM) exactly stick together in both regions and form unique U-shaped nodal surfaces while they are fully gapped beside these regions. Figure 2b,d presents the element-projected density of states (DOS) for ScH_3 and LuH_3, respectively. It is evident that the bands near the Fermi level are mainly contributed by the d orbitals of Sc/Lu atoms that are hybridized with the s orbitals of H atoms (the Lu f orbitals make no contribution to the bands near the Fermi level). The hybridization strength is the strongest in ScH_3 as it has a small lattice constant,[94,95] which causes flatness of the degenerate bands around Γ, resulting in a wider U-shape of the degenerate bands in ScH_3 (see Figure 2a,c). With flat bands, many allowed states occupy almost the same energy levels, resulting in a high or diverging DOS, a characteristic feature of vHs.[96−98] It is evident that the vHs is present in the DOS of ScH_3 and LuH_3 (indicated by the magenta arrows in Figure 2b,d), demonstrat-

https://doi.org/10.1021/acsomega.3c00207
ACS Omega 2023, 8, 9607−9613

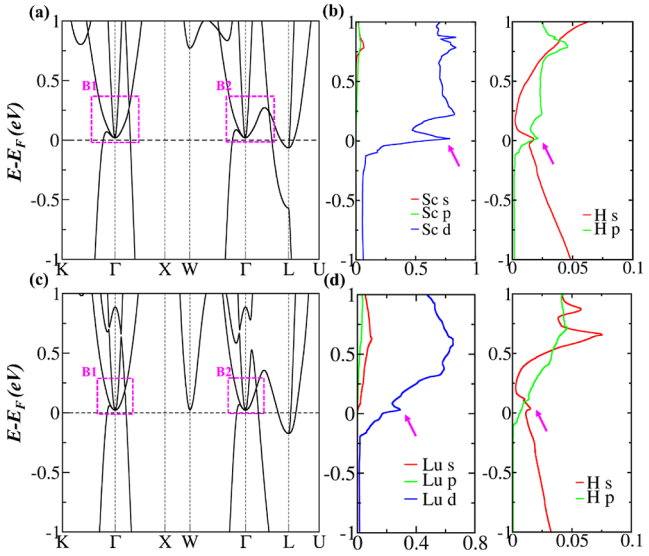

Figure 2. Electronic band structures and orbital projected DOS for (a,b) ScH_3 and (c,d) LuH_3 using the SCAN functional. The high-symmetry k points are given in Figure 1b. The magenta arrows in (b,d) point to the diverging DOS.

ing that superconductivity emerges in these materials due to the presence of flat bands near the Fermi level.

To confirm the shape of topological nodal surfaces, the 3D energy bands with Γ-point at the middle for ScH_3 and LuH_3 are computed without SOC in Figure 3a,b, respectively. There

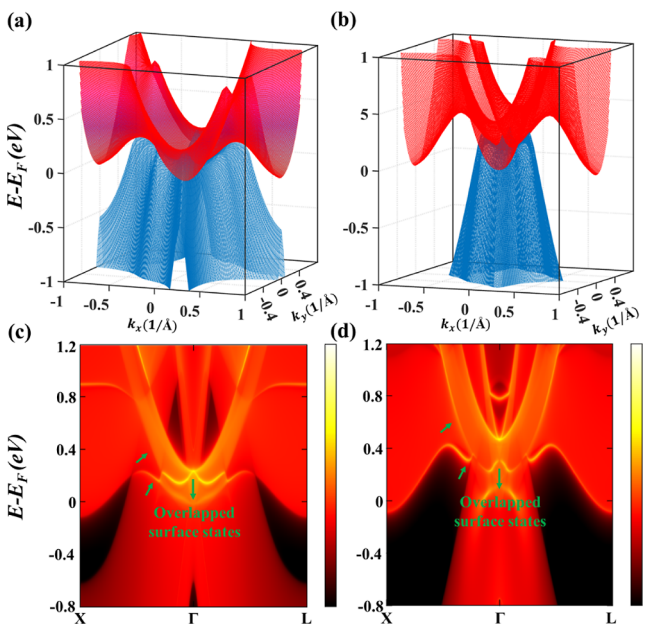

Figure 3. 3D band structures under SCAN without SOC for (a) ScH_3 and (b) LuH_3 near the nodal lines form in the vicinity of the Fermi level. The calculated (100) surface band structures for (c) ScH_3 and (d) LuH_3 along the projected X–Γ–Z k-path without SOC.

is a clear U-shaped overlap between VBM and CBM around Γ, which corresponds to the nodal surfaces formed due to the band touching points in ScH_3 and LuH_3. Besides, an important characteristic of topological materials is their novel surface states. TIs exhibit helical surface states, while materials with topological nodal lines usually exhibit drumhead-like surfaces without SOC. However, the surface states of NSSMs are not evident since, to the best of our knowledge, they have never been reported. Figure 3c,d displays the calculated surface energy spectra for ScH_3 and LuH_3, respectively, in the absence of SOC. Interestingly, the surface spectra of both NSSM materials contain two drumhead-like surface states pointed by green arrows which are entirely overlapped around Γ and get separated as we move away from Γ in both directions. These findings provide an insight into how NSSM's surface states can appear, which can be used to identify their nodal surface states in experiments.

Next, we examine how SOC affects the electronic and topological properties of ScH_3 and LuH_3. Figure 4 shows the

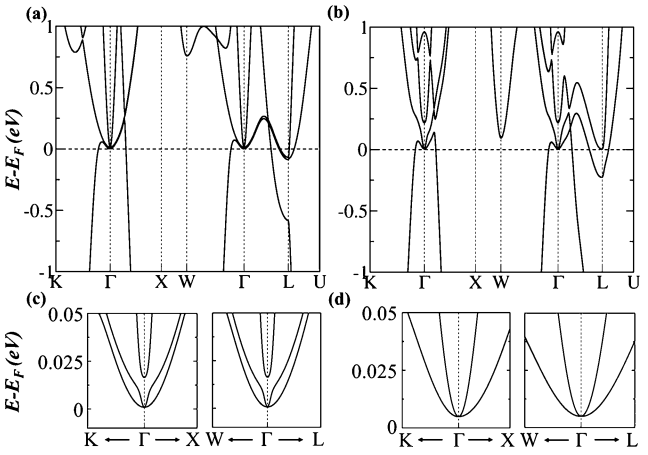

Figure 4. Calculated electronic band structures with SOC for (a) ScH_3 and (b) LuH_3 using the SCAN functional. Panels (c,d) are the zoomed-in images for the low-energy bands along K–Γ–X and W–Γ–L, showing two Dirac points at Γ for both ScH_3 and LuH_3, respectively.

electronic band structures of ScH_3 and LuH_3 with SOC. Clearly, the 2D nodal surfaces have been removed, and a small gap between VBM and CBM has appeared along K–Γ, Γ–X and W–Γ, Γ–L, as shown in zoomed-in plots in Figure 4c,d. However, in both materials, the VBM and CBM remain connected at Γ and form Dirac points. Furthermore, the dispersion of these Dirac points is quadratic[83] rather than linear, and they are robust against SOC. In fact, these Dirac points only appear in the presence of SOC.

To support the findings, 3D energy bands of ScH_3 and LuH_3 are depicted in Figure 5a,b, respectively, demonstrating a clear crossing between the VBM and CBM at Γ. Following that, the surface states of ScH_3 and LuH_3 are investigated under SOC (see Figure 5c,d). The two drumhead surface states, which were previously overlapped in the absence of SOC, are now completely gapped, as expected in type-I NSSMs.[40] Besides, the bulk states are mixed with each other around Γ, and the locations of bulk Dirac cones could be faintly visible as indicated by the green dots.

Our simulations show both superconducting and topological properties for ScH_3 and LuH_3. Since these two materials have been realized experimentally, we suggest they be used as a platform to explore this combination of properties for applications in spintronics and topological quantum computation. Our theoretical findings suggest that the NSSM states and their unique properties are more likely to be observed in ScH_3

https://doi.org/10.1021/acsomega.3c00207
ACS Omega 2023, 8, 9607−9613

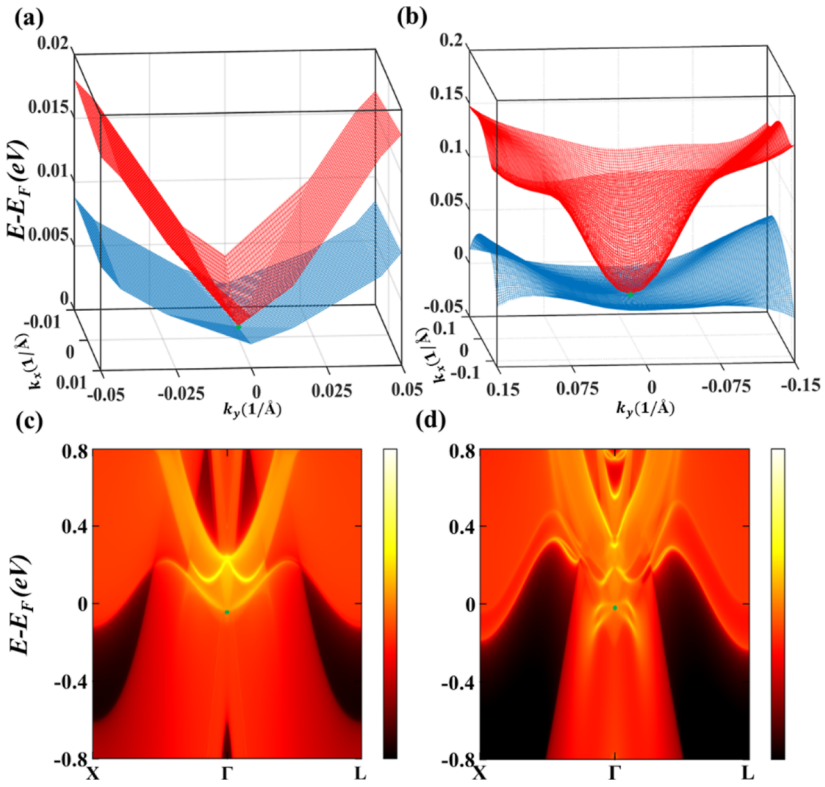

Figure 5. 3D band structures under SCAN with SOC for (a) ScH_3 and (b) LuH_3 near the Dirac points form in the vicinity of the Fermi level. (c) Surface band structures calculated along the projected $X-\Gamma-Z$ k-path for ScH_3 and (d) LuH_3 with SOC. The position of bulk Dirac points is denoted by the green points.

since the SOC-induced gap is extremely small around its nodal surfaces.

CONCLUSIONS

In summary, on the basis of first-principles calculations, we predicted the existence of U-shaped nodal surface states in two superconductors, ScH_3 and LuH_3, in the absence of SOC. The nodal surfaces are formed by a continuous overlap of VBM and CBM around Γ and exhibit drum-head-like surface states that have not been reported before. With the inclusion of SOC, the nodal surfaces weakly split and transform into quadratic Dirac points. Besides, both materials contain vHss, proving their superconductive nature. Considering the fact that the SOC-induced gaps around the nodal surfaces are small, especially in the ScH_3 case, these materials are promising to serve as good candidates to study both NSSMs and quadratic Dirac semimetal states and also provide a platform to explore the coexistence of topology and superconductivity in NSSMs.

ASSOCIATED CONTENT

Supporting Information

The Supporting Information is available free of charge at https://pubs.acs.org/doi/10.1021/acsomega.3c00207.

Electronic band structures and partial density of states of ScH_3 and LuH_3 without SOC at 140 and 122 GPa pressure, respectively; 3D band structures and surface states of ScH_3 and LuH_3 at 140 and 122 GPa, respectively, without SOC; electronic band structures of ScH3 at 140 GPa and LuH_3 at 122 GPa with SOC; 3D band structures and surface states for ScH_3 at 140 GPa and LuH_3 at 122 GPa with SOC; and the zoomed-in view of 3D band structures of ScH_3 and LuH_3 at ambient pressure without SOC near the Dirac points (PDF)

AUTHOR INFORMATION

Corresponding Author

Ali Sufyan − *Applied Physics, Division of Materials Science, Department of Engineering Sciences and Mathematics, Luleå University of Technology, Luleå SE-97187, Sweden;* orcid.org/0000-0002-4507-2759; Email: ali.sufyan@associated.ltu.se

Author

J. Andreas Larsson − *Applied Physics, Division of Materials Science, Department of Engineering Sciences and Mathematics, Luleå University of Technology, Luleå SE-97187, Sweden;* orcid.org/0000-0003-3455-2877

Complete contact information is available at: https://pubs.acs.org/10.1021/acsomega.3c00207

Author Contributions

A.S. performed the calculations; A.S. and J.A.L. analyzed the results. Both authors reviewed the manuscript.

Notes

The authors declare no competing financial interest.

The data that support the findings of this study are available from the corresponding author upon reasonable request.

ACKNOWLEDGMENTS

The fruitful discussion with Shahid Sattar is greatly acknowledged. The authors thank the Knut and Alice Wallenberg

https://doi.org/10.1021/acsomega.3c00207
ACS Omega 2023, 8, 9607−9613

Foundation and Kempestiftelserna for financial support. The computations were enabled by resources provided by the Swedish National Infrastructure for Computing (SNIC) at HPC2N and NSC partially funded by the Swedish Research Council through grant agreement no. 2018-05973.

REFERENCES

(1) Hasan, M. Z.; Kane, C. L. Colloquium: Topological Insulators. *Rev. Mod. Phys.* **2010**, *82*, 3045−3067.
(2) Bansil, A.; Lin, H.; Das, T. Colloquium: Topological Band Theory. *Rev. Mod. Phys.* **2016**, *88*, 021004.
(3) Yan, B.; Felser, C. Topological Materials: Weyl Semimetals. *Annu. Rev. Condens. Matter Phys.* **2017**, *8*, 337−354.
(4) Kane, C. L.; Mele, E. J. Quantum Spin Hall Effect in Graphene. *Phys. Rev. Lett.* **2005**, *95*, 226801.
(5) Kane, C. L.; Mele, E. J. Z2Topological Order and the Quantum Spin Hall Effect. *Phys. Rev. Lett.* **2005**, *95*, 146802.
(6) Xia, Y.; Qian, D.; Hsieh, D.; Wray, L.; Pal, A.; Lin, H.; Bansil, A.; Grauer, D.; Hor, Y. S.; Cava, R. J.; Hasan, M. Z. Observation of a Large-Gap Topological-Insulator Class with a Single Dirac Cone on the Surface. *Nat. Phys.* **2009**, *5*, 398−402.
(7) Bernevig, B. A.; Hughes, T. L.; Zhang, S.-C. Quantum Spin Hall Effect and Topological Phase Transition in HgTe Quantum Wells. *Science* **2006**, *314*, 1757−1761.
(8) Fu, L.; Kane, C. L.; Mele, E. J. Topological Insulators in Three Dimensions. *Phys. Rev. Lett.* **2007**, *98*, 106803.
(9) Roy, R. Topological Phases and the Quantum Spin Hall Effect in Three Dimensions. *Phys. Rev. B: Condens. Matter Mater. Phys.* **2009**, *79*, 195322.
(10) Chen, Y. L.; Analytis, J. G.; Chu, J.-H.; Liu, Z. K.; Mo, S.-K.; Qi, X. L.; Zhang, H. J.; Lu, D. H.; Dai, X.; Fang, Z.; Zhang, S. C.; Fisher, I. R.; Hussain, Z.; Shen, Z.-X. Experimental Realization of a Three-Dimensional Topological Insulator, Bi2Te3. *Science* **2009**, *325*, 178−181.
(11) Hsieh, D.; Qian, D.; Wray, L.; Xia, Y.; Hor, Y. S.; Cava, R. J.; Hasan, M. Z. A Topological Dirac Insulator in a Quantum Spin Hall Phase. *Nature* **2008**, *452*, 970−974.
(12) Sufyan, A.; Maghirang, A. B.; Macam, G.; Huang, Z.-Q.; Hsu, C.-H.; Chuang, F.-C. Electronic and Topological Band Evolution of VB-Group Transitionmetal Monocarbides M2C (M=V, Nb, or Ta) Bulk and Monolayer. *Mater. Today Commun.* **2022**, *32*, 103875.
(13) Sattar, S.; Larsson, J. A. Tunable Electronic Properties and Large Rashba Splittings Found in Few-Layer Bi2Se3/PtSe2 Van Der Waals Heterostructures. *ACS Appl. Electron. Mater.* **2020**, *2*, 3585−3592.
(14) Zhang, H.; Liu, C.-X.; Qi, X.-L.; Dai, X.; Fang, Z.; Zhang, S.-C. Topological Insulators in Bi2Se3, Bi2Te3 and Sb2Te3 with a Single Dirac Cone on the Surface. *Nat. Phys.* **2009**, *5*, 438−442.
(15) Yan, W.-K.; Zhang, A.-B.; Yi, L.-J. Influence of spherical inclusions on effective thermoelectric properties of thermoelectric composite materials. *Chin. Phys. B* **2020**, *29*, 057301.
(16) Lu, Y.; Xu, W.; Zeng, M.; Yao, G.; Shen, L.; Yang, M.; Luo, Z.; Pan, F.; Wu, K.; Das, T.; He, P.; Jiang, J.; Martin, J.; Feng, Y. P.; Lin, H.; Wang, X. Topological Properties Determined by Atomic Buckling in Self-Assembled Ultrathin Bi(110). *Nano Lett.* **2015**, *15*, 80−87.
(17) Hasan, M. Z.; Xu, S.-Y.; Bian, G. Topological Insulators, Topological Superconductors and Weyl Fermion Semimetals: Discoveries, Perspectives and Outlooks. *Phys. Scripta* **2015**, *T164*, 014001.
(18) Yang, S. A. Dirac and Weyl Materials: Fundamental Aspects and Some Spintronics Applications. *SPIN* **2016**, *06*, 1640003.
(19) Balents, L. Weyl Electrons Kiss. *Physics* **2011**, *4*, 36.
(20) Burkov, A. A. Weyl Metals. *Annu. Rev. Condens. Matter Phys.* **2018**, *9*, 359−378.
(21) Young, S. M.; Zaheer, S.; Teo, J. C. Y.; Kane, C. L.; Mele, E. J.; Rappe, A. M. Dirac Semimetal in Three Dimensions. *Phys. Rev. Lett.* **2012**, *108*, 140405.
(22) Fang, C.; Weng, H.; Dai, X.; Fang, Z. Topological Nodal Line Semimetals*. *Chin. Phys. B* **2016**, *25*, 117106.
(23) Wang, Z.; Sun, Y.; Chen, X.-Q.; Franchini, C.; Xu, G.; Weng, H.; Dai, X.; Fang, Z. Dirac semimetal and topological phase transitions inA3Bi (A=Na, K, Rb). *Phys. Rev. B: Condens. Matter Mater. Phys.* **2012**, *85*, 195320.
(24) Wang, Z.; Weng, H.; Wu, Q.; Dai, X.; Fang, Z. Three-dimensional Dirac semimetal and quantum transport in Cd3As2. *Phys. Rev. B: Condens. Matter Mater. Phys.* **2013**, *88*, 125427.
(25) Yang, B.-J.; Nagaosa, N. Classification of Stable Three-Dimensional Dirac Semimetals with Nontrivial Topology. *Nat. Commun.* **2014**, *5*, 4898.
(26) Borisenko, S.; Gibson, Q.; Evtushinsky, D.; Zabolotnyy, V.; Büchner, B.; Cava, R. J. Experimental Realization of a Three-Dimensional Dirac Semimetal. *Phys. Rev. Lett.* **2014**, *113*, 027603.
(27) Burkov, A. A.; Balents, L. Weyl Semimetal in a Topological Insulator Multilayer. *Phys. Rev. Lett.* **2011**, *107*, 127205.
(28) Huang, S.-M.; Xu, S.-Y.; Belopolski, I.; Lee, C.-C.; Chang, G.; Wang, B.; Alidoust, N.; Bian, G.; Neupane, M.; Zhang, C.; Jia, S.; Bansil, A.; Lin, H.; Hasan, M. Z. A Weyl Fermion Semimetal with Surface Fermi Arcs in the Transition Metal Monopnictide TaAs Class. *Nat. Commun.* **2015**, *6*, 7373.
(29) Singh, B.; Sharma, A.; Lin, H.; Hasan, M. Z.; Prasad, R.; Bansil, A. Topological Electronic Structure and Weyl Semimetal in the TlBiSe${}_{2}$ Class of Semiconductors. *Phys. Rev. B: Condens. Matter Mater. Phys.* **2012**, *86*, 115208.
(30) Hua, C.; Li, S.; Xu, Z.-A.; Zheng, Y.; Yang, S. A.; Lu, Y. Tunable Topological Energy Bands in 2D Dialkali-Metal Monoxides. *Adv. Sci.* **2020**, *7*, 1901939.
(31) Burkov, A. A.; Hook, M. D.; Balents, L. Topological Nodal Semimetals. *Phys. Rev. B: Condens. Matter Mater. Phys.* **2011**, *84*, 235126.
(32) Weng, H.; Liang, Y.; Xu, Q.; Yu, R.; Fang, Z.; Dai, X.; Kawazoe, Y. Topological Node-Line Semimetal in Three-Dimensional Graphene Networks. *Phys. Rev. B: Condens. Matter Mater. Phys.* **2015**, *92*, 045108.
(33) Mullen, K.; Uchoa, B.; Glatzhofer, D. T. Line of Dirac Nodes in Hyperhoneycomb Lattices. *Phys. Rev. Lett.* **2015**, *115*, 026403.
(34) Chen, Y.; Xie, Y.; Yang, S. A.; Pan, H.; Zhang, F.; Cohen, M. L.; Zhang, S. Nanostructured Carbon Allotropes with Weyl-like Loops and Points. *Nano Lett.* **2015**, *15*, 6974−6978.
(35) Fang, C.; Chen, Y.; Kee, H.-Y.; Fu, L. Topological Nodal Line Semimetals with and without Spin-Orbital Coupling. *Phys. Rev. B: Condens. Matter Mater. Phys.* **2015**, *92*, 081201.
(36) Yu, R.; Weng, H.; Fang, Z.; Dai, X.; Hu, X. Topological Node-Line Semimetal and Dirac Semimetal State in Antiperovskite Cu3PdN. *Phys. Rev. Lett.* **2015**, *115*, 036807.
(37) Kim, Y.; Wieder, B. J.; Kane, C. L.; Rappe, A. M. Dirac Line Nodes in Inversion-Symmetric Crystals. *Phys. Rev. Lett.* **2015**, *115*, 036806.
(38) Li, R.; Ma, H.; Cheng, X.; Wang, S.; Li, D.; Zhang, Z.; Li, Y.; Chen, X.-Q. Dirac Node Lines in Pure Alkali Earth Metals. *Phys. Rev. Lett.* **2016**, *117*, 096401.
(39) Li, S.; Yu, Z.-M.; Liu, Y.; Guan, S.; Wang, S.-S.; Zhang, X.; Yao, Y.; Yang, S. A. Type-II Nodal Loops: Theory and Material Realization. *Phys. Rev. B* **2017**, *96*, 081106.
(40) Wu, W.; Liu, Y.; Li, S.; Zhong, C.; Yu, Z.-M.; Sheng, X.-L.; Zhao, Y. X.; Yang, S. A. Nodal Surface Semimetals: Theory and Material Realization. *Phys. Rev. B* **2018**, *97*, 115125.
(41) Xiao, M.; Ye, L.; Qiu, C.; He, H.; Liu, Z.; Fan, S. Experimental Demonstration of Acoustic Semimetal with Topologically Charged Nodal Surface. *Sci. Adv.* **2020**, *6*, No. eaav2360.
(42) Zhong, C.; Chen, Y.; Xie, Y.; Yang, S. A.; Cohen, M. L.; Zhang, S. B. Towards Three-Dimensional Weyl-Surface Semimetals in Graphene Networks. *Nanoscale* **2016**, *8*, 7232−7239.
(43) Liang, Q.-F.; Zhou, J.; Yu, R.; Wang, Z.; Weng, H. Node-Surface and Node-Line Fermions from Nonsymmorphic Lattice Symmetries. *Phys. Rev. B* **2016**, *93*, 085427.

https://doi.org/10.1021/acsomega.3c00207
ACS Omega 2023, 8, 9607−9613

(44) Zhang, X.; Yu, Z.-M.; Zhu, Z.; Wu, W.; Wang, S.-S.; Sheng, X.-L.; Yang, S. A. Nodal loop and nodal surface states in the Ti3Al family of materials. *Phys. Rev. B* **2018**, *97*, 235150.
(45) Li, S.; Liu, Y.; Wang, S.-S.; Yu, Z.-M.; Guan, S.; Sheng, X.-L.; Yao, Y.; Yang, S. A. Nonsymmorphic-symmetry-protected hourglass Dirac loop, nodal line, and Dirac point in bulk and monolayer X3SiTe6 (X = Ta, Nb). *Phys. Rev. B* **2018**, *97*, 045131.
(46) Yang, T.; Zhang, X. Nearly Flat Nodal Surface States in Pseudo-One-Dimensional Molybdenum Monochalcogenides X(MoS)3 (X = K, Rb, and Cs). *J. Mater. Chem. C* **2020**, *8*, 9046−9054.
(47) Yang, T.; Jin, L.; Liu, Y.; Zhang, X.; Wang, X. Spin-polarized type-II nodal loop and nodal surface states in hexagonal compounds XTiO2 (X = Li, Na, K, Rb). *Phys. Rev. B* **2021**, *103*, 235140.
(48) Khan, M. R.; Bu, K.; Wang, J.-T.; Chen, C. Topological nodal surface semimetal states in SrSX3 compounds (X=As,Sb,Bi). *Phys. Rev. B* **2022**, *105*, 245152.
(49) Nayak, C.; Simon, S. H.; Stern, A.; Freedman, M.; Das Sarma, S. Non-Abelian Anyons and Topological Quantum Computation. *Rev. Mod. Phys.* **2008**, *80*, 1083−1159.
(50) Qi, X.-L.; Zhang, S.-C. Topological Insulators and Superconductors. *Rev. Mod. Phys.* **2011**, *83*, 1057−1110.
(51) Alicea, J. New Directions in the Pursuit of Majorana Fermions in Solid State Systems. *Rep. Prog. Phys.* **2012**, *75*, 076501.
(52) Sato, M.; Ando, Y. Topological Superconductors: A Review. *Rep. Prog. Phys.* **2017**, *80*, 076501.
(53) Ando, Y.; Fu, L. Topological Crystalline Insulators and Topological Superconductors: From Concepts to Materials. *Annu. Rev. Condens. Matter Phys.* **2015**, *6*, 361−381.
(54) Wray, L. A.; Xu, S.-Y.; Xia, Y.; Hor, Y. S.; Qian, D.; Fedorov, A. V.; Lin, H.; Bansil, A.; Cava, R. J.; Hasan, M. Z. Observation of Topological Order in a Superconducting Doped Topological Insulator. *Nat. Phys.* **2010**, *6*, 855−859.
(55) Hosur, P.; Ghaemi, P.; Mong, R. S. K.; Vishwanath, A. Majorana Modes at the Ends of Superconductor Vortices in Doped Topological Insulators. *Phys. Rev. Lett.* **2011**, *107*, 097001.
(56) Sasaki, S.; Kriener, M.; Segawa, K.; Yada, K.; Tanaka, Y.; Sato, M.; Ando, Y. Topological Superconductivity inCuxBi2Se3. *Phys. Rev. Lett.* **2011**, *107*, 217001.
(57) Asaba, T.; Lawson, B. J.; Tinsman, C.; Chen, L.; Corbae, P.; Li, G.; Qiu, Y.; Hor, Y. S.; Fu, L.; Li, L. Rotational Symmetry Breaking in a Trigonal Superconductor Nb-doped Bi2Se3. *Phys. Rev. X* **2017**, *7*, 011009.
(58) Zhu, J.; Zhang, J. L.; Kong, P. P.; Zhang, S. J.; Yu, X. H.; Zhu, J. L.; Liu, Q. Q.; Li, X.; Yu, R. C.; Ahuja, R.; Yang, W. G.; Shen, G. Y.; Mao, H. K.; Weng, H. M.; Dai, X.; Fang, Z.; Zhao, Y. S.; Jin, C. Q. Superconductivity in Topological Insulator Sb2Te3 Induced by Pressure. *Sci. Rep.* **2013**, *3*, 2016.
(59) Wang, H.; Wang, H.; Liu, H.; Lu, H.; Yang, W.; Jia, S.; Liu, X.-J.; Xie, X. C.; Wei, J.; Wang, J. Observation of Superconductivity Induced by a Point Contact on 3D Dirac Semimetal Cd3As2 Crystals. *Nat. Mater.* **2016**, *15*, 38−42.
(60) Yin, J.-X.; Wu, Z.; Wang, J.-H.; Ye, Z.-Y.; Gong, J.; Hou, X.-Y.; Shan, L.; Li, A.; Liang, X.-J.; Wu, X.-X.; Li, J.; Ting, C.-S.; Wang, Z.-Q.; Hu, J.-P.; Hor, P.-H.; Ding, H.; Pan, S. H. Observation of a Robust Zero-Energy Bound State in Iron-Based Superconductor Fe(Te,Se). *Nat. Phys.* **2015**, *11*, 543−546.
(61) Wang, D.; Kong, L.; Fan, P.; Chen, H.; Zhu, S.; Liu, W.; Cao, L.; Sun, Y.; Du, S.; Schneeloch, J.; Zhong, R.; Gu, G.; Fu, L.; Ding, H.; Gao, H.-J. Evidence for Majorana Bound States in an Iron-Based Superconductor. *Science* **2018**, *362*, 333−335.
(62) Zhang, P.; Yaji, K.; Hashimoto, T.; Ota, Y.; Kondo, T.; Okazaki, K.; Wang, Z.; Wen, J.; Gu, G. D.; Ding, H.; Shin, S. Observation of Topological Superconductivity on the Surface of an Iron-Based Superconductor. *Science* **2018**, *360*, 182−186.
(63) Wu, X.; Qin, S.; Liang, Y.; Fan, H.; Hu, J. Topological characters in Fe(Te1−xSex) thin films. *Phys. Rev. B* **2016**, *93*, 115129.
(64) Xu, G.; Lian, B.; Tang, P.; Qi, X.-L.; Zhang, S.-C. Topological Superconductivity on the Surface of Fe-Based Superconductors. *Phys. Rev. Lett.* **2016**, *117*, 047001.
(65) Zhang, P.; Wang, Z.; Wu, X.; Yaji, K.; Ishida, Y.; Kohama, Y.; Dai, G.; Sun, Y.; Bareille, C.; Kuroda, K.; Kondo, T.; Okazaki, K.; Kindo, K.; Wang, X.; Jin, C.; Hu, J.; Thomale, R.; Sumida, K.; Wu, S.; Miyamoto, K.; Okuda, T.; Ding, H.; Gu, G. D.; Tamegai, T.; Kawakami, T.; Sato, M.; Shin, S. Multiple Topological States in Iron-Based Superconductors. *Nat. Phys.* **2019**, *15*, 41−47.
(66) Wang, Z.; Zhang, P.; Xu, G.; Zeng, L. K.; Miao, H.; Xu, X.; Qian, T.; Weng, H.; Richard, P.; Fedorov, A. V.; Ding, H.; Dai, X.; Fang, Z. Topological nature of the FeSe0.5Te0.5 superconductor. *Phys. Rev. B: Condens. Matter Mater. Phys.* **2015**, *92*, 115119.
(67) Sakintuna, B.; Lamaridarkrim, F.; Hirscher, M. Metal Hydride Materials for Solid Hydrogen Storage: A Review☆. *Int. J. Hydrogen Energy* **2007**, *32*, 1121−1140.
(68) Smith, J. S.; Desgreniers, S.; Tse, J. S.; Klug, D. D. High-Pressure Phase Transition Observed in Barium Hydride. *J. Appl. Phys.* **2007**, *102*, 043520.
(69) Tse, J. S.; Yao, Y.; Tanaka, K. Novel Superconductivity in Metallic SnH4 under High Pressure. *Phys. Rev. Lett.* **2007**, *98*, 117004.
(70) Jin, X.; Meng, X.; He, Z.; Ma, Y.; Liu, B.; Cui, T.; Zou, G.; Mao, H. Superconducting High-Pressure Phases of Disilane. *Proc. Natl. Acad. Sci.* **2010**, *107*, 9969−9973.
(71) Shamp, A.; Zurek, E. Superconducting High-Pressure Phases Composed of Hydrogen and Iodine. *J. Phys. Chem. Lett.* **2015**, *6*, 4067−4072.
(72) Duan, D.; Liu, Y.; Ma, Y.; Shao, Z.; Liu, B.; Cui, T. Structure and Superconductivity of Hydrides at High Pressures. *Natl. Sci. Rev.* **2017**, *4*, 121−135.
(73) Ashcroft, N. W. Hydrogen Dominant Metallic Alloys: High Temperature Superconductors? *Phys. Rev. Lett.* **2004**, *92*, 187002.
(74) Liu, H.; Naumov, I. I.; Geballe, Z. M.; Somayazulu, M.; Tse, J. S.; Hemley, R. J. Dynamics and Superconductivity in Compressed Lanthanum Superhydride. *Phys. Rev. B* **2018**, *98*, 100102.
(75) Somayazulu, M.; Ahart, M.; Mishra, A. K.; Geballe, Z. M.; Baldini, M.; Meng, Y.; Struzhkin, V. V.; Hemley, R. J. Evidence for Superconductivity above 260 K in Lanthanum Superhydride at Megabar Pressures. *Phys. Rev. Lett.* **2019**, *122*, 027001.
(76) Liu, H.; Naumov, I. I.; Hoffmann, R.; Ashcroft, N. W.; Hemley, R. J. Potential High-Tc Superconducting Lanthanum and Yttrium Hydrides at High Pressure. *Proc. Natl. Acad. Sci.* **2017**, *114*, 6990−6995.
(77) Drozdov, A. P.; Kong, P. P.; Minkov, V. S.; Besedin, S. P.; Kuzovnikov, M. A.; Mozaffari, S.; Balicas, L.; Balakirev, F. F.; Graf, D. E.; Prakapenka, V. B.; Greenberg, E.; Knyazev, D. A.; Tkacz, M.; Eremets, M. I. Superconductivity at 250 K in Lanthanum Hydride under High Pressures. *Nature* **2019**, *569*, 528−531.
(78) Struzhkin, V.; Li, B.; Ji, C.; Chen, X.-J.; Prakapenka, V.; Greenberg, E.; Troyan, I.; Gavriliuk, A.; Mao, H. Superconductivity in La and Y Hydrides: Remaining Questions to Experiment and Theory. *Matter Radiat. Extremes* **2020**, *5*, 028201.
(79) Chen, W.; Semenok, D. V.; Huang, X.; Shu, H.; Li, X.; Duan, D.; Cui, T.; Oganov, A. R. High-Temperature Superconducting Phases in Cerium Superhydride with a Tc up to 115 K below a Pressure of 1 Megabarr. *Phys. Rev. Lett.* **2021**, *127*, 117001.
(80) Troyan, I. A.; Semenok, D. V.; Kvashnin, A. G.; Sadakov, A. V.; Sobolevskiy, O. A.; Pudalov, V. M.; Ivanova, A. G.; Prakapenka, V. B.; Greenberg, E.; Gavriliuk, A. G.; Lyubutin, I. S.; Struzhkin, V. V.; Bergara, A.; Errea, I.; Bianco, R.; Calandra, M.; Mauri, F.; Monacelli, L.; Akashi, R.; Oganov, A. R. Anomalous High-Temperature Superconductivity in YH6. *Adv. Mater.* **2021**, *33*, 2006832.
(81) Kong, P.; Minkov, V. S.; Kuzovnikov, M. A.; Drozdov, A. P.; Besedin, S. P.; Mozaffari, S.; Balicas, L.; Balakirev, F. F.; Prakapenka, V. B.; Chariton, S.; Knyazev, D. A.; Greenberg, E.; Eremets, M. I. Superconductivity up to 243 K in the Yttrium-Hydrogen System under High Pressure. *Nat. Commun.* **2021**, *12*, 5075.
(82) Shao, M.; Chen, S.; Chen, W.; Zhang, K.; Huang, X.; Cui, T. Superconducting ScH3 and LuH3 at Megabar Pressures. *Inorg. Chem.* **2021**, *60*, 15330−15335.
(83) Tian, L.; Liu, Y.; Meng, W.; Zhang, X.; Dai, X.; Liu, G. Spin−Orbit Coupling-Determined Topological Phase: Topological Insulator

https://doi.org/10.1021/acsomega.3c00207
ACS Omega 2023, 8, 9607−9613

and Quadratic Dirac Semimetals. *J. Phys. Chem. Lett.* **2020**, *11*, 10340−10347.
(84) Hohenberg, P.; Kohn, W. Inhomogeneous Electron Gas. *Phys. Rev.* **1964**, *136*, B864−B871.
(85) Kresse, G.; Joubert, D. From Ultrasoft Pseudopotentials to the Projector Augmented-Wave Method. *Phys. Rev. B: Condens. Matter Mater. Phys.* **1999**, *59*, 1758−1775.
(86) Kresse, G.; Furthmüller, J. Efficient Iterative Schemes for Ab Initio Total-Energy Calculations Using a Plane-Wave Basis Set. *Phys. Rev. B: Condens. Matter Mater. Phys.* **1996**, *54*, 11169−11186.
(87) Kresse, G.; Hafner, J. Ab Initio Molecular Dynamics for Liquid Metals. *Phys. Rev. B: Condens. Matter Mater. Phys.* **1993**, *47*, 558−561.
(88) Perdew, J. P.; Burke, K.; Ernzerhof, M. Generalized Gradient Approximation Made Simple. *Phys. Rev. Lett.* **1996**, *77*, 3865−3868.
(89) Monkhorst, H. J.; Pack, J. D. Special Points for Brillouin-Zone Integrations. *Phys. Rev. B: Solid State* **1976**, *13*, 5188−5192.
(90) Sun, J.; Ruzsinszky, A.; Perdew, J. P. Strongly Constrained and Appropriately Normed Semilocal Density Functional. *Phys. Rev. Lett.* **2015**, *115*, 036402.
(91) Wang, V.; Xu, N.; Liu, J.-C.; Tang, G.; Geng, W.-T. VASPKIT: A User-Friendly Interface Facilitating High-Throughput Computing and Analysis Using VASP Code. *Comput. Phys. Commun.* **2021**, *267*, 108033.
(92) Marzari, N.; Vanderbilt, D. Maximally Localized Generalized Wannier Functions for Composite Energy Bands. *Phys. Rev. B: Condens. Matter Mater. Phys.* **1997**, *56*, 12847−12865.
(93) Wu, Q.; Zhang, S.; Song, H.-F.; Troyer, M.; Soluyanov, A. A. WannierTools: An Open-Source Software Package for Novel Topological Materials. *Comput. Phys. Commun.* **2018**, *224*, 405−416.
(94) Sattar, S.; Islam, M. F.; Canali, C. M. Monolayer MnX and Janus XMnY (X,Y=S , Se, Te): A family of two-dimensional antiferromagnetic semiconductors. *Phys. Rev. B* **2022**, *106*, 085410.
(95) Sattar, S.; Singh, N.; Schwingenschlögl, U. Silicene on Monolayer PtSe2: From Strong to Weak Binding via NH3 Intercalation. *ACS Appl. Mater. Interfaces* **2018**, *10*, 4266−4270.
(96) Noda, K.; Inaba, K.; Yamashita, M. Magnetism in the Three-Dimensional Layered Lieb Lattice: Enhanced Transition Temperature via Flat-Band and Van Hove Singularities. *Phys. Rev. A* **2015**, *91*, 063610.
(97) Honerkamp, C.; Salmhofer, M. Magnetic and Superconducting Instabilities of the Hubbard Model at the Van Hove Filling. *Phys. Rev. Lett.* **2001**, *87*, 187004.
(98) Villaos, R. A. B.; Crisostomo, C. P.; Huang, Z.-Q.; Huang, S.-M.; Padama, A. A. B.; Albao, M. A.; Lin, H.; Chuang, F.-C. Thickness Dependent Electronic Properties of Pt Dichalcogenides. *npj 2D Mater. Appl.* **2019**, *3*, 2.

https://doi.org/10.1021/acsomega.3c00207
ACS Omega 2023, 8, 9607−9613